(18)

21

Fracture in Pressure Vessels

E. S. FOLIAS

A survey of existing exact solutions describing the stress distribution around a crack tip in an initially curved sheet is made, and a method for estimating the stress-intensity factors of more complicated geometries is discussed.

With a Dugdale-type model, the size of the plastic zone ahead of the crack tip is estimated, and a fracture criterion incorporating geometry and plasticity corrections is suggested. This criterion predicts failures in pressurized vessels of arbitrary shape by knowing only shell geometry, material properties, and crack size. A comparison with some of the experimental data in existing literature substantiates the validity of the fracture criterion and its potential use.

INTRODUCTION

It is well known that initially curved sheets containing through cracks have a reduced resistance to fracture initiation. Consequently, a crack in the walls of a pressure vessel can severely reduce the strength of the structure and can cause sudden failure at a nominal tensile stress less than the material yield strength. Therefore, to ensure the integrity of a structure, the designer must be cognizant of the relation that exists among fracture load, flaw shape and size, matrial properties, and structural geometry. A relation of this kind is called a fracture criterion and can be derived by the application of the theory of fracture mechanics.

For the derivation of a fracture criterion two ingredients are necessary:

From THIN-SHELL STRUCTURES: Theory, Experiment, and Design, Y.C. Fung and E.E. Sechler, editors.

a knowledge of the stress distribution due to the presence of a crack, and an energy balance for crack initiation. Accordingly, in the first part of this chapter, a review of past work on initially curved sheets dealing with the stress distribution in the vicinity of a crack is given, and in the second part a fracture criterion with which one may predict fracture in pressure vessels is discussed. Finally, a comparison of the theoretically predicted values with some of the existing experimental data is presented.

STRESS DISTRIBUTION IN THE VICINITY OF A CRACK

General Theory

In the following, we shall consider bending and stretching of thin shallow shells,† as illustrated in Fig. 1 and described by the traditional two-dimensional

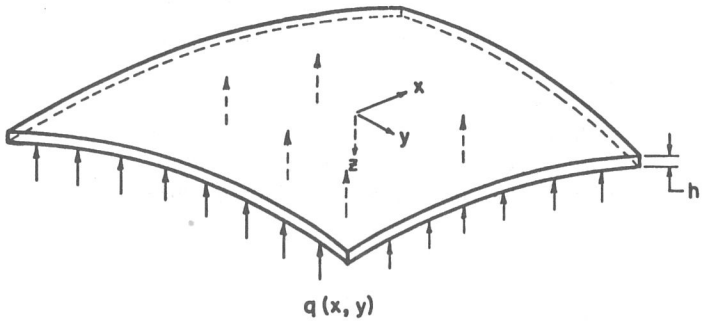

Figure 1 Initially curved sheet.

linear theory. Such a theory is appropriate in view of the "thinness" of the shell. We shall limit our consideration to elastic, isotropic, homogeneous, constant thickness, shallow segments of shells, subjected to small deformations and strains.

The basic variables in the theory of shallow shells are the displacement function $w(x, y)$ in the direction of the z axis (see Fig. 1) and a stress function $F(x, y)$ which represents the stress resultants tangent to the middle surface of the shell. Following Marguerre (1938), the coupled differential equations governing w and F, with x and y as rectangular Cartesian coordinates of the base plane (see Fig. 1), are given by

† According to Ogibalov (1966), a shell will be called *shallow* if the least radius of curvature is greater by one order of magnitude than the linear dimensions, i.e., $L/R \leq 0.1$, and *thin* if $h/R \leq 0.01$.

$$\nabla^4 F = Eh\left[2\frac{\partial^2 w_0}{\partial x\,\partial y}\frac{\partial^2 w}{\partial x\,\partial y} - \frac{\partial^2 w_0}{\partial x^2}\frac{\partial^2 w}{\partial y^2} - \frac{\partial^2 w_0}{\partial y^2}\frac{\partial^2 w}{\partial x^2}\right] \tag{1a}$$

$$D\nabla^4 w = -q - 2\frac{\partial^2 F}{\partial x\,\partial y}\frac{\partial^2 w_0}{\partial x\,\partial y} + \frac{\partial^2 F}{\partial x^2}\frac{\partial^2 w_0}{\partial y^2} + \frac{\partial^2 F}{\partial y^2}\frac{\partial^2 w_0}{\partial x^2} \tag{2a}$$

where $w_0(x, y)$ describes the initial shape of the shell in reference to that of a flat plate.

Formulation of the stress problem

Let us consider a portion of a thin, shallow shell, of constant thickness h, subjected to an internal pressure $q(x, y)$ and containing a crack of length $2c$ (see Fig. 2). Our problem is to find two functions $F(x, y)$ and $w(x, y)$

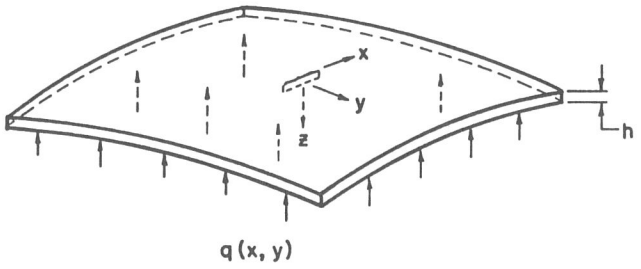

Figure 2 Initially curved sheet containing a finite line crack.

satisfying the differential equations (1a) and (2a), and appropriate boundary conditions. We require that (1) on the faces of the crack, the normal moment, equivalent shear, and normal and tangential membrane forces vanish, and (2) away from the crack, the appropriate loading and support conditions are satisfied.

In treating this problem, it is convenient to seek the solution in two parts, the *undisturbed* or *particular* solution which satisfies Eqs. (1a) and (2a) and the loading and support conditions but leaves residual forces along the crack†, and the *complementary* solution which precisely nullifies these residuals and offers no contribution far away from the crack.

It is evident from Eqs. (1a) and (2a) that a theoretical attack of the general problem for an arbitrary initial curvature presents formidable mathematical complexities. However, for spherical and cylindrical shells, exact solutions have been obtained in an asymptotic form. For other more complicated shells results can be obtained by a proper superposition of these two solutions.

† For more details, see Folias (1964a).

Spherical shell. For a shallow spherical shell the radius of curvature remains constant in all directions; therefore,

$$\frac{\partial^2 w_0}{\partial x\,\partial y} = 0; \qquad \frac{\partial^2 w_0}{\partial x^2} = \frac{\partial^2 w_0}{\partial y^2} = \frac{1}{R} \tag{3a}$$

Substituting Eqs. (3a) into Eqs. (1a) and (2a), one obtains Reissner's equations

$$\frac{Eh}{R}\nabla^2 w + \nabla^4 F = 0 \tag{1b}$$

$$\nabla^4 w - \frac{1}{RD}\nabla^2 F = -\frac{q}{D} \tag{2b}$$

For a spherical cap containing a crack of finite length $2c$ at the apex (see Fig. 3), the author (Folias, 1965a) has reduced the problem to the solution

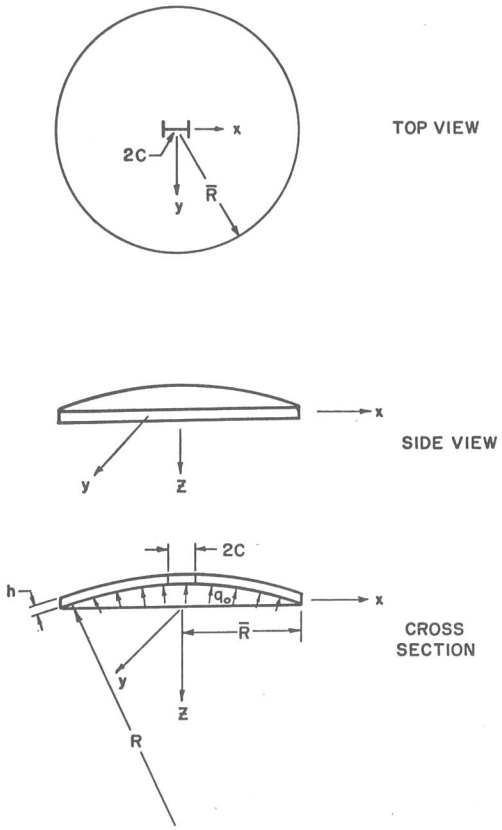

Figure 3 Geometrical configuration of a pressurized spherical cap.

of two coupled singular integral equations. The solution was sought in a power series of λ, where λ was given by

$$\lambda \equiv \left(\frac{Ehc^4}{R^2D}\right)^{1/4} \equiv \{12(1-\nu^2)\}^{1/4}\left\{\frac{R}{h}\right\}^{1/2}\frac{c}{R} \equiv \{12(1-\nu^2)\}^{1/4}\frac{c}{(Rh)^{1/2}} \tag{4}$$

Furthermore, the author has shown (Folias, 1964a) that for λ less than a calculated bound the series does converge to the exact solution.

It is clear from Eq. (4) that λ is small for large ratios of R/h and small crack lengths. As practical matter, if one considers crack lengths less than one-tenth of the periphery, i.e., $2c < (2\pi R/10)$, and for $(R/h) < 10^3$ a corresponding upper bound for λ can be obtained, i.e., $\lambda < 20$. For most practical cases we have $0 \leq \lambda < 3$. Consequently, an asymptotic expansion for small λ is justifiable.

Without getting into the details, the stress distribution around the crack tip for a symmetrical loading† is

Extensional stresses—through the thickness:

$$\sigma_x^{(e)} = P_s^{(e)}\left(\frac{c}{2r}\right)^{1/2}\left(\frac{3}{4}\cos\frac{\theta}{2} + \frac{1}{4}\cos\frac{5\theta}{2}\right) + 0(r^0) \tag{5}$$

$$\sigma_y^{(e)} = P_s^{(e)}\left(\frac{c}{2r}\right)^{1/2}\left(\frac{5}{4}\cos\frac{\theta}{2} - \frac{1}{4}\cos\frac{5\theta}{2}\right) + 0(r^0) \tag{6}$$

$$\tau_{xy}^{(e)} = P_s^{(e)}\left(\frac{c}{2r}\right)^{1/2}\left(-\frac{1}{4}\sin\frac{\theta}{2} + \frac{1}{4}\sin\frac{5\theta}{2}\right) + 0(r^0) \tag{7}$$

Bending stresses—on the "tension side" of the shell:

$$\sigma_x^{(b)} = P_s^{(b)}\left(\frac{c}{2r}\right)^{1/2}\left(-\frac{3-3\nu}{4}\cos\frac{\theta}{2} - \frac{1-\nu}{4}\cos\frac{5\theta}{2}\right) + 0(r^0) \tag{8}$$

$$\sigma_y^{(b)} = P_s^{(b)}\left(\frac{c}{2r}\right)^{1/2}\left(\frac{11+5\nu}{4}\cos\frac{\theta}{2} + \frac{1-\nu}{4}\cos\frac{5\theta}{2}\right) + 0(r^0) \tag{9}$$

$$\tau_{xy}^{(b)} = P_s^{(b)}\left(\frac{c}{2r}\right)^{1/2}\left(-\frac{7+\nu}{4}\sin\frac{\theta}{2} - \frac{1-\nu}{4}\sin\frac{5\theta}{2}\right) + 0(r^0) \tag{10}$$

where

$$P_s^{(e)} = \bar{\sigma}^{(e)}\left\{1 + \frac{3\pi}{32}\lambda^2\right\} + \bar{\sigma}^{(b)}\frac{(\lambda^2)(1-\nu^2)^{1/2}}{3^{1/2}(4-\nu_0)}\left\{\frac{7}{32} + \frac{3}{8}\left(\gamma + \ln\frac{\lambda}{4}\right)\right\} + 0(\lambda^4 \ln\lambda) \tag{11a}$$

† For antisymmetric loadings, see Folias, 1964a.

and

$$P_s^{(b)} = -\bar{\sigma}^{(e)} \frac{\lambda^2(3^{1/2})}{(1-\nu^2)^{1/2}(4-\nu_0)} \left\{ \frac{8-7\nu_0}{32} + \frac{4-3\nu_0}{8} \left(\gamma + \ln \frac{\lambda}{4} \right) \right\} - \frac{\bar{\sigma}^{(b)}}{4-\nu_0} \left\{ 1 + \frac{4-3\nu_0}{4-\nu_0} \frac{\pi\lambda^2}{32} \right\} + 0(\lambda^4 \ln \lambda) \tag{12a}$$

It should be emphasized that the stress coefficients in Eqs. (11a) and (12a) contain terms only up to $0(\lambda^2)$; hence their use is limited to small values of the parameter λ, in particular $\lambda < 1$. If one wishes to know the stress coefficients for large values of λ, it is necessary to consider higher-order terms in order to guarantee convergence. This matter was investigated by Erdogan and Kibler (1969), who, with the aid of a computer, were able to extend the results of Folias (1965a) to $\lambda \leq 5.5$. Thus, for a Poisson's ratio of $\frac{1}{3}$, an alternative form of the stress coefficients good up to $\lambda \leq 5.5$ is

$$P_s^{(e)} = \bar{\sigma}^{(e)} A_s^{(e)} - 0.54\bar{\sigma}^{(b)} a_s^{(e)} \tag{13a}$$

$$P_s^{(b)} = 1.81\bar{\sigma}^{(e)} a_s^{(b)} - 0.30\bar{\sigma}^{(b)} A_s^{(b)} \tag{14a}$$

where the coefficients $A_s^{(e)}$, $A_s^{(b)}$, $a_s^{(e)}$, and $a_s^{(b)}$ are functions of λ and are given in Table 1 or by Figs. 4 through 7.

TABLE 1
Sphere

λ	$A_s^{(e)}$	$A_s^{(b)}$	$a_s^{(e)}$	$a_s^{(b)}$
0.2	1.0112	1.0020	0.00842	0.00611
0.4	1.0422	1.0070	0.02249	0.01693
0.6	1.0887	1.0137	0.03749	0.02919
0.8	1.1479	1.0211	0.05202	0.04186
1.0	1.2174	1.0287	0.06557	0.05448
1.2	1.2956	1.0364	0.07799	0.06685
1.4	1.3812	1.0439	0.08935	0.07886
1.6	1.4731	1.0512	0.09964	0.09045
1.8	1.5706	1.0583	0.10895	0.10155
2.0	1.6729	1.0652	0.11740	0.11216
2.2	1.7795	1.0718	0.12519	0.12223
2.4	1.8899	1.0783	0.13228	0.13172
2.6	2.0038	1.0845	0.13876	0.14058
2.8	2.1208	1.0905	0.14475	0.14879
3.0	2.2408	1.0964	0.15030	0.15630
3.25	2.3947	1.1035	0.15668	0.16463
3.50	2.5526	1.1103	0.16260	0.17172
3.75	2.7143	1.1170	0.1681	0.17751
4.00	2.8796	1.1233	0.1732	0.18194
4.25	3.0485	1.1297	0.1780	0.18483
4.50	3.2208	1.1357	0.1826	0.18644
5.00	3.5750	1.1470	0.1905	0.18493
5.50	3.9446	1.1580	0.2000	0.17802

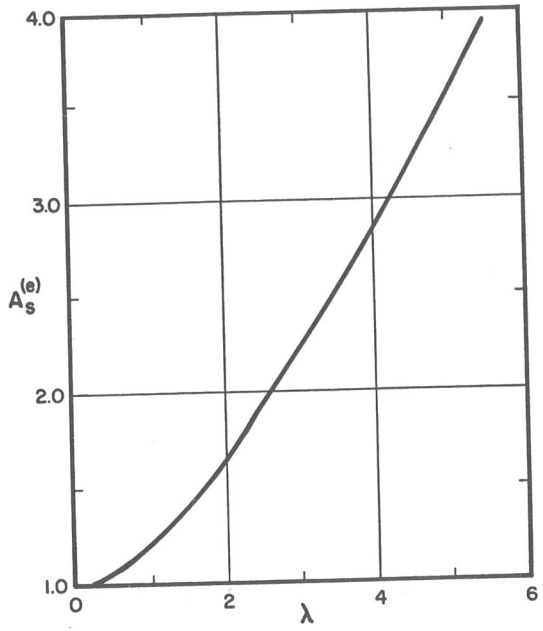

Figure 4 Stress coefficient for a sphere. (According to Erdogan and Kibler, 1969.)

$$A_s^{(e)} = I_s$$

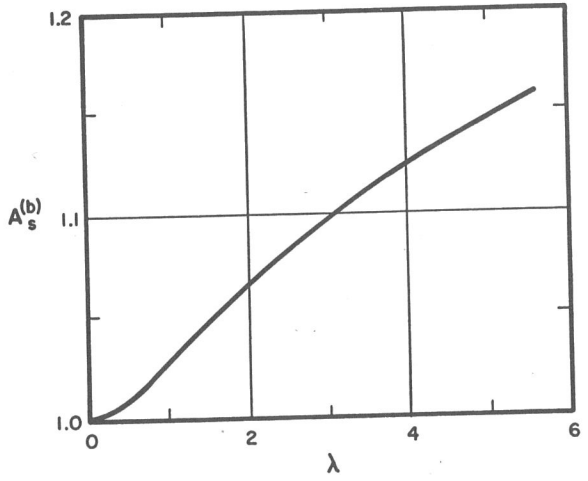

Figure 5 Stress coefficient for a sphere. (According to Erdogan and Kibler, 1969.)

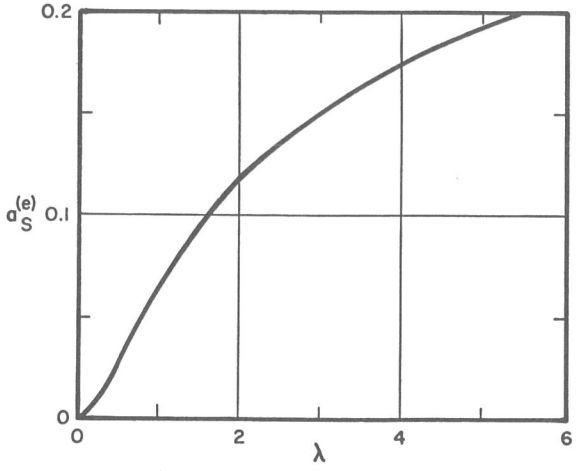

Figure 6 Stress coefficient for a sphere. (According to Erdogan and Kibler, 1969.)

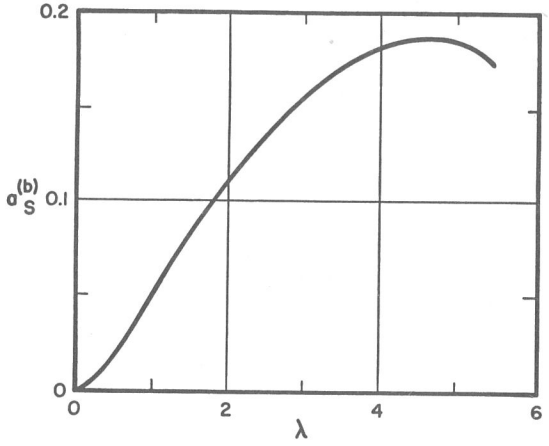

Figure 7 Stress coefficient for a sphere. (According to Erdogan and Kibler, 1969.)

$$a_s^{(b)} = 0.54 J_s$$

Flat plate. A flat plate represents a degenerative case of a spherical cap when the radius becomes infinite; therefore,

$$\frac{\partial^2 w_0}{\partial x\, \partial y} = \frac{\partial^2 w_0}{\partial x^2} = \frac{\partial^2 w_0}{\partial y^2} = 0 \tag{3b}$$

Substituting Eq. (3b) into Eqs. (1a) and (2a), one recovers the classic equa-

tions for a flat plate, i.e.,

$$\nabla^4 F = 0 \tag{1c}$$

$$\nabla^4 w = -\frac{q}{D} \tag{2c}$$

The problem of a flat plate containing a finite crack subjected to a lateral load has been investigated by many authors for various types of loadings. The solution, however, can also be obtained from that of the spherical cap by letting $R \longrightarrow \infty$ or $\lambda \longrightarrow 0$. Thus the stresses around the crack tip are given precisely by Eqs. (5)–(10), where the stress coefficients now are

$$P_p^{(e)} = \bar{\sigma}^{(e)} \tag{11b}$$

$$P_p^{(b)} = -\frac{\bar{\sigma}^{(b)}}{4 - \nu_0} \tag{12b}$$

Cylindrical shell. For a shallow cylindrical shell, one of the principal radii of curvatures is infinite, while the other one is constant; therefore,

$$\frac{\partial^2 w_0}{\partial x\, \partial y} = \frac{\partial^2 w_0}{\partial x^2} = 0; \qquad \frac{\partial^2 w_0}{\partial y^2} = \frac{1}{R} \tag{3c}$$

Substituting Eq. (3c) into Eqs. (1a) and (2a), one recovers the equations for a shallow cylindrical shell, i.e.,

$$\frac{Eh}{R}\frac{\partial^2 w}{\partial x^2} + \nabla^4 F = 0 \tag{1d}$$

$$\nabla^4 w - \frac{1}{RD}\frac{\partial^2 F}{\partial x^2} = -\frac{q}{D} \tag{2d}$$

Two cases of special interest immediately come to mind: an axial and a peripheral crack. Due to the mathematical complexities of this problem, Sechler and Williams (1959) suggested an approximate method of solution based on the behavior of a beam on an elastic foundation and hence were able to obtain a reasonable agreement with the experimental results. The author, however, using the same method of solution as in Folias (1965a), was able to investigate this problem in a more sophisticated manner, and the details for an axial and a peripheral crack (see Fig. 8) can be found in Folias, 1965b and 1967.

Subsequently, there have been two more theoretical analyses of this problem, the axial crack by Copley and Sanders (1969) and the peripheral crack by Duncan and Sanders (1969). Their method of solution consists of the application of the Fourier integral theorem leading to the derivation of two

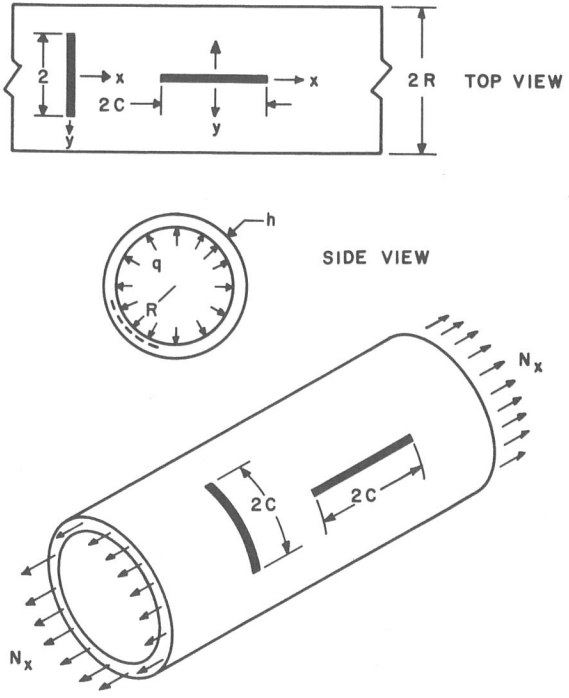

Figure 8 Geometry and coordinates of an axially cracked cylinder shell under uniform axial extension N_x and internal pressure q_o.

coupled singular integral equations (different in form from the author's), which in turn are approximated to high accuracy by matrix equations and are solved by the use of a computer. Their results were derived for zero *applied bending load*, i.e., $\bar{\sigma}^{(b)} = 0$, and for Poisson's ratio, $\nu = 0.32$.

Again omitting the mathematical details (see Folias, 1965b and 1967), the stresses around the crack tip are given also by Eqs. (5)–(10), where the stress coefficients now are

For an axial crack:

$$P_{c,a}^{(e)} = \bar{\sigma}^{(e)}\left\{1 + \frac{5\pi\lambda^2}{64}\right\} + \bar{\sigma}^{(b)}\frac{\lambda^2(1-\nu^2)^{1/2}}{3^{1/2}(4-\nu_0)}\left\{\frac{42-37\nu_0}{96\nu_0} + \frac{6-5\nu_0}{16\nu_0} \cdot \left(\gamma + \ln\frac{\lambda}{8}\right)\right\} + 0(\lambda^4 \ln\lambda), \qquad \lambda < 1 \tag{11c}$$

$$P_{c,a}^{(b)} = -\bar{\sigma}^{(e)}\frac{\lambda^2(3^{1/2})}{(1-\nu^2)^{1/2}(4-\nu_0)}\left\{\frac{42-37\nu_0}{96} + \frac{6-5\nu_0}{16}\left(\gamma + \ln\frac{\lambda}{8}\right)\right\} - \frac{\bar{\sigma}^{(b)}}{4-\nu_0}\left\{1 + \frac{12\nu_0 - 5\nu_0^2 - 8}{(4-\nu_0)\nu_0}\frac{\pi\lambda^2}{64}\right\} + 0(\lambda^4 \ln\lambda), \qquad \lambda < 1 \tag{12c}$$

or the alternative numerical form (Erdogan and Kibler, 1969) valid for $\nu = \frac{1}{3}$

and $\lambda \leq 8$,

$$P_{c,a}^{(e)} = \bar{\sigma}^{(e)} A_{c,a}^{(e)} - 0.54\bar{\sigma}^{(b)} a_{c,a}^{(e)} \tag{13b}$$

$$P_{c,a}^{(b)} = 1.81\bar{\sigma}^{(e)} a_{c,a}^{(b)} - 0.30\bar{\sigma}^{(b)} A_{c,a}^{(b)} \tag{14b}$$

Here again the coefficients $A_{c,a}^{(e)}$, $A_{c,a}^{(b)}$, $a_{c,a}^{(e)}$, and $a_{c,a}^{(b)}$ are functions of λ and are given in Table 2 or by Figs. 9, 10, and 11. In Fig. 11 we compare, for $\bar{\sigma}^{(b)} = 0$,

TABLE 2
Cylinder

λ	$A_{c,a}^{(e)}$	$A_{c,a}^{(b)}$	$a_{c,a}^{(e)}$	$a_{c,a}^{(b)}$
0.2	1.0096	0.99816	0.006161	0.00410
0.4	1.0371	0.99340	0.01695	0.01124
0.6	1.0795	0.98660	0.02897	0.01902
0.8	1.1344	0.97846	0.04107	0.02659
1.0	1.1993	0.96946	0.05283	0.03359
1.2	1.2723	0.95986	0.06406	0.03985
1.4	1.3519	0.94993	0.07473	0.04529
1.6	1.4367	0.93976	0.08482	0.04990
1.8	1.5256	0.92956	0.09435	0.05368
2.0	1.6177	0.91936	0.1033	0.05664
2.2	1.7122	0.90923	0.1118	0.05883
2.4	1.8085	0.89926	0.1198	0.06018
2.6	1.9060	0.88940	0.1273	0.06090
2.8	2.0045	0.87970	0.1344	0.06083
3.0	2.1035	0.87023	0.1410	0.06014
3.25	2.2276	0.85863	0.1488	0.05832
3.50	2.3519	0.84740	0.1551	0.05549
3.75	2.4761	0.83643	0.1629	0.05172
4.00	2.5999	0.82440	0.1691	0.04700
4.25	2.7232	0.81542	0.1750	0.04154
4.50	2.8459	0.80539	0.1803	0.03512
5.00	3.0895	0.78616	0.1903	0.02012
5.50	3.3303	0.76832	0.2005	0.00234
6.00	3.5681	0.75079	0.2068	0.02222
6.50	3.8029	0.73446	0.2137	0.04130
7.00	4.0347	0.71879	0.2200	0.06622
7.50	4.2637	0.7080	0.2255	0.09350
8.00	4.4895	0.6897	0.2306	0.12279

the results of Erdogan and Kibler (1969) with those of Copley and Sanders (1969). The comparison is very good up to $\lambda < 3.3$, beyond which Copley's results become somewhat higher.

For a peripheral crack:

$$P_{c,p}^{(e)} = \bar{\sigma}^{(e)}\left\{1 + \frac{\pi\lambda^2}{64}\right\} + \bar{\sigma}^{(b)}\frac{\lambda^2(1-\nu^2)^{1/2}}{3^{1/2}(4-\nu_0)}\left\{\frac{(1+\nu)}{32\nu_0} + \frac{(1+\nu)}{16\nu_0}\left(\gamma + \ln\frac{\lambda}{8}\right)\right\}$$
$$+ 0(\lambda^4 \ln \lambda), \qquad \lambda < 2.5 \tag{11d}$$

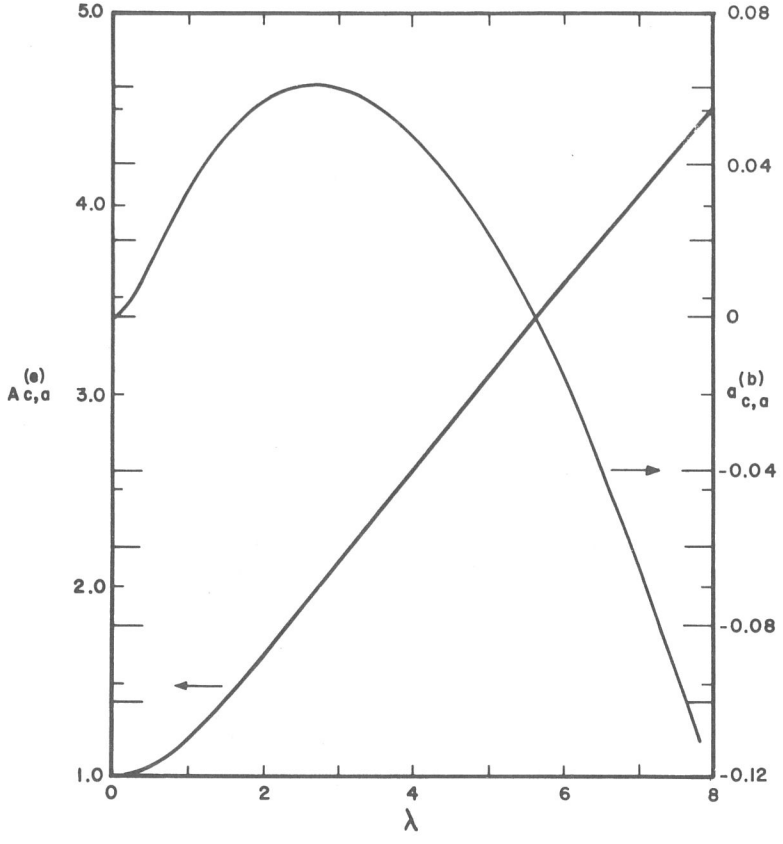

Figure 9 Stress coefficient for a cylinder.

$$A_{c,a}^{(e)} = I_{c,a} \qquad a_{c,a}^{(b)} = 0.54 J_{c,a}$$

$$P_{c,p}^{(b)} = -\bar{\sigma}^{(e)} \frac{\lambda^2 (3^{1/2})}{(1-\nu^2)^{1/2}(4-\nu_0)} \left\{ \frac{1+\nu}{32} + \frac{1+\nu}{16} \left(\gamma + \ln \frac{\lambda}{8} \right) \right\}$$
$$- \frac{\bar{\sigma}^{(b)}}{4-\nu_0} \left\{ 1 - \frac{5+2\nu+\nu^2}{(4-\nu_0)\nu_0} \frac{\pi\lambda^2}{64} \right\} + 0(\lambda^4 \ln \lambda), \qquad \lambda < 2.5 \qquad (12d)$$

Here again the stress coefficients are valid only for small values of the parameter λ, and for $\lambda > 2.5$ one must consider higher-order terms. Figure 12 gives Duncan's results for $\nu = 0.32$ and $\bar{\sigma}^{(b)} = 0$. Notice that for small λs ($\lambda < 2.5$) the stress coefficients given by Eqs. (11d) and (12d) and Duncan's results are identical.

For an arbitrarily oriented crack† (see Fig. 13):

† Approximate stress intensity factors; for derivation, see Folias, 1969b. It should be emphasized here that the angular distribution associated with $\bar{\tau}^{(e)}$ and $\bar{\tau}^{(b)}$ is not that given by Eqs. (5)–(10), but similar. See Folias (1964a) for the exact solution of the antisymmetric problem in a spherical shell.

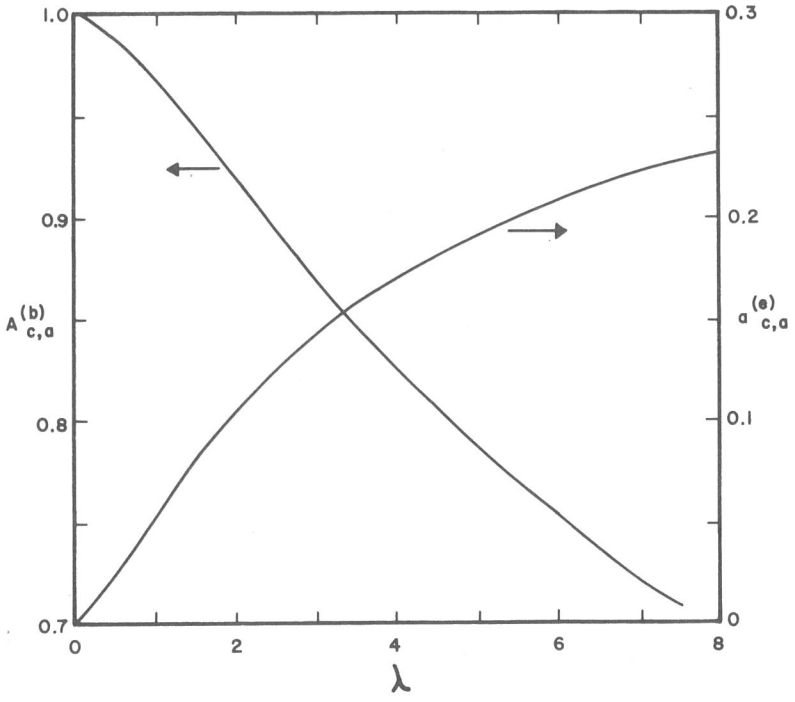

Figure 10 Stress coefficient for a cylinder. (According to Erdogan and Kibler, 1969.)

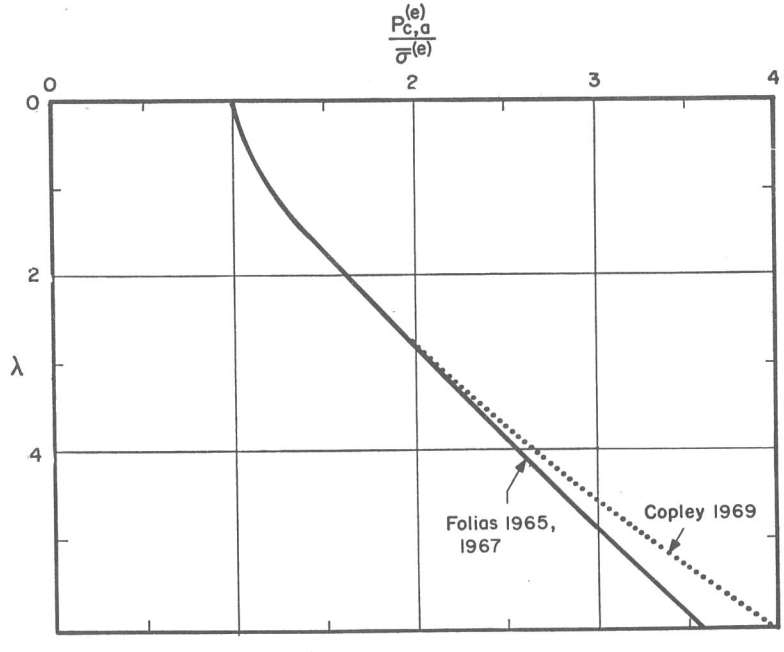

Figure 11 Comparison of the two methods for the stress coefficient of a cylindrical shell containing an axial crack.

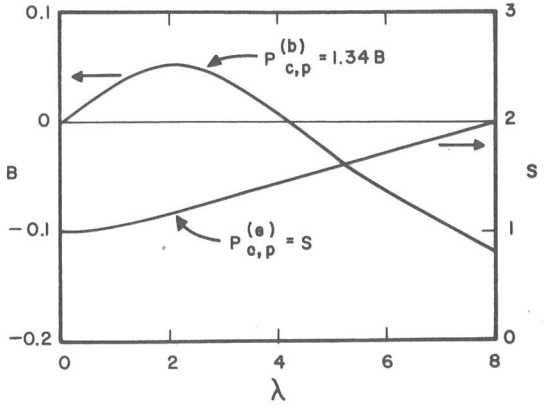

Figure 12 Duncan's stress coefficients for a cylindrical shell containing a peripheral crack.

$$S = I_{c,p};\quad B = 0.75J_{c,p}$$

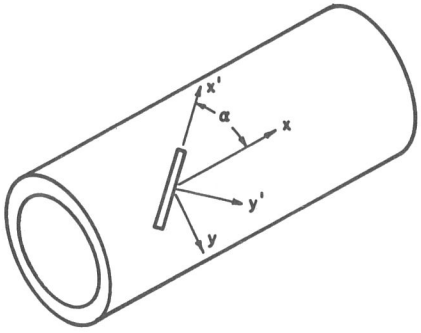

Figure 13 Coordinates of an arbitrary oriented crack in a cylindrical shell.

$$\begin{aligned}
P^{(e)}_{c,\alpha} = {} & \bar{\sigma}^{(e)}\left\{1 + \frac{(5\cos^2\alpha + \sin^2\alpha)\pi\lambda^2}{64}\right\} \pm \bar{\tau}^{(e)}\left\{1 + 5^{1/2}\frac{\pi\lambda^2}{64}\sin 2\alpha\right\} \\
& + \bar{\sigma}^{(b)}\frac{\lambda^2(1-\nu^2)}{3^{1/2}(4-\nu_0)}\left\{\left[\frac{42-37\nu_0}{96\nu_0} + \frac{6-5\nu_0}{16\nu_0}\left(\gamma + \ln\frac{\lambda\cos\alpha}{8}\right)\right]\cos^2\alpha\right. \\
& \left. + \left[\frac{1+\nu}{32\nu_0} + \frac{1+\nu}{16\nu_0}\left(\gamma + \ln\frac{\lambda\sin\alpha}{8}\right)\right]\sin^2\alpha\right\} \\
& \pm \bar{\tau}^{(b)}\frac{\lambda^2(1-\nu^2)^{1/2}}{3^{1/2}(4-\nu_0)}\left\{\frac{42-37\nu_0}{96\nu_0} + \frac{6-5\nu_0}{16\nu_0}\left(\gamma + \ln\frac{\lambda\cos\alpha}{8}\right)\right\}^{1/2} \\
& \cdot \left\{\frac{(1+\nu)}{32\nu_0} + \frac{(1+\nu)}{16\nu_0}\left(\gamma + \ln\frac{\lambda\sin\alpha}{8}\right)\right\}^{1/2}\sin 2\alpha \\
& + 0(\lambda^4\ln\lambda), \qquad \lambda < 1
\end{aligned} \tag{11e}$$

$$P^{(b)}_{c,\alpha} = -\bar{\sigma}^{(e)} \frac{\lambda^2(3^{1/2})}{(1-\nu^2)^{1/2}(4-\nu_0)} \left\{ \left[\frac{42-37\nu_0}{96} + \frac{6-5\nu_0}{16} \right.\right.$$
$$\left. \cdot \left(\gamma + \ln \frac{\lambda \cos\alpha}{8} \right) \right] \cos^2\alpha + \left[\frac{1+\nu}{32} + \frac{1+\nu}{16} \left(\gamma + \ln \frac{\lambda \sin\alpha}{8} \right) \right] \sin^2\alpha \Bigg\}$$
$$+ \bar{\tau}^{(e)} \frac{\lambda^2(3^{1/2})}{(1-\nu^2)^{1/2}(4-\nu_0)} \left\{ \left[\frac{42-37\nu_0}{96} + \frac{6-5\nu_0}{16} \left(\gamma + \ln \frac{\lambda \cos\alpha}{8} \right) \right]^{1/2} \right.$$
$$\left. \cdot \left[\frac{1+\nu}{32} + \frac{1+\nu}{16} \left(\gamma + \ln \frac{\lambda \sin\alpha}{8} \right) \right]^{1/2} \right\} \sin 2\alpha$$
$$- \frac{\bar{\sigma}^{(b)}}{4-\nu_0} \left\{ 1 - \frac{(1+2\nu+5\nu^2)\cos^2\alpha + (5+2\nu+\nu^2)\sin^2\alpha}{(4-\nu_0)\nu_0} \frac{\pi\lambda^2}{64} \right\}$$
$$\mp \frac{\bar{\tau}^{(b)}}{4-\nu_0} \left\{ 1 + \frac{(5\nu_0^2 - 12\nu_0 + 8)^{1/2}(\nu^2+2\nu+5)^{1/2}}{(4-\nu_0)\nu_0} \frac{\pi\lambda^2}{64} \sin 2\alpha \right\}$$
$$+ 0(\lambda^4 \ln \lambda), \qquad \lambda < 1 \tag{12e}$$

An alternative form valid only for $\bar{\sigma}^{(b)} = 0$, $\nu = \frac{1}{3}$, and $\lambda \leq 8$ is

$$P^{(e)}_{c,\alpha} = \bar{\sigma}^{(e)} \{ 1 + (\tilde{P}^{(e)}_{c,a} - 1)|_{\lambda=\lambda\cos\alpha} + (\tilde{P}^{(e)}_{c,p} - 1)|_{\lambda=\lambda\sin\alpha} \}$$
$$\pm \bar{\tau}^{(e)} \{ 1 + (\tilde{P}^{(e)}_{c,a}|_{\lambda=\lambda\cos\alpha} - 1)^{1/2} (\tilde{P}^{(e)}_{c,p}|_{\lambda=\lambda\sin\alpha} - 1)^{1/2} \} \tag{13c}$$

$$\tilde{P}^{(b)}_{c,\alpha} = -\bar{\sigma}^{(e)} \{ \tilde{P}^{(b)}_{c,a}|_{\lambda=\lambda\cos\alpha} + \tilde{P}^{(b)}_{c,p}|_{\lambda=\lambda\sin\alpha} \}$$
$$\mp \bar{\tau}^{(e)} \{ \tilde{P}^{(b)}_{c,a}|_{\lambda=\lambda\cos\alpha})^{1/2} (\tilde{P}^{(b)}_{c,p}|_{\lambda=\lambda\sin\alpha})^{1/2} \} \tag{14c}$$

where $\tilde{P}^{(\ )} \equiv P^{(\ )}/\bar{\sigma}^{(e)}$.

Approximate stress factors for other shell geometries. If one chooses the coordinate axes x and y such that they are parallel to the principal radii of curvature†, then

$$\frac{\partial^2 w_0}{\partial x\, \partial y} = 0, \qquad \frac{\partial^2 w_0}{\partial x^2} = \frac{1}{R_x}, \qquad \frac{\partial^2 w_0}{\partial y^2} = \frac{1}{R_y} \tag{3d}$$

where R_x and R_y are principal radii of curvatures in the x and y directions, respectively. Substituting Eq. (3d) into Eqs. (1a) and (2a), one finds

$$Eh\left[\frac{1}{R_y} \frac{\partial^2 w}{\partial x^2} + \frac{1}{R_x} \frac{\partial^2 w}{\partial y^2} \right] + \nabla^4 F = 0 \tag{1e}$$

$$\nabla^4 w - \frac{1}{D}\left[\frac{1}{R_y} \frac{\partial^2 F}{\partial x^2} + \frac{1}{R_x} \frac{\partial^2 F}{\partial y^2} \right] = -\frac{q}{D} \tag{2e}$$

Inasmuch as the complementary solution or the perturbed solution presents contributions only in the immediate vicinity of the crack tip, one

† In a more general case, when they are not parallel, Eqs. (1e) and (2e) will contain additional terms of the form $(\partial^2 w/\partial x\, \partial y)$ and $(\partial^2 F/\partial x\, \partial y)$. For the angular distribution of this case, see the footnote on p. 494.

may consider—at least locally—the principal radii of curvatures to be constants. Thus assuming that the crack is parallel to one of the principal axes, e.g., along the x- axis, one may hypothesize that the stress coefficients depend primarily on the curvatures that one observes as he travels parallel and perpendicular to the crack. Consequently, one may estimate the stress coefficients by a proper superposition of the results of an axial and a peripheral crack in a cylindrical shell. In particular, for $\bar{\sigma}^{(b)} = 0$,

$$P^{(e)} \approx \bar{\sigma}^{(e)}\left\{1 + \frac{\pi\lambda_x^2}{64} + \frac{5\pi\lambda_y^2}{64}\right\} \tag{11f}$$

$$P^{(b)} \approx -\sigma^{(e)}\frac{3^{1/2}}{(1-\nu^2)^{1/2}(4-\nu_0)}\left\{\frac{42-37\nu_0}{96}\lambda_x^2 + \frac{6-5\nu_0}{16}\lambda_y^2\left(\gamma + \ln\frac{\lambda_y}{8}\right)\right.$$
$$\left. + \frac{1+\nu}{32}\lambda_x^2 + \frac{1+\nu}{16}\lambda_x^2\left(\gamma + \ln\frac{\lambda_x}{8}\right)\right\} + 0(\lambda \ln \lambda) \qquad \lambda < 1 \tag{12f}$$

or the alternative numerical form valid for $\nu = \frac{1}{3}$ and $\lambda \leq 8$

$$P^{(e)} \approx \bar{\sigma}^{(e)}\{1 + (P_{c,a}^{(e)} - 1)|_{\lambda=\lambda_y} + (P_{c,p}^{(e)} - 1)|_{\lambda=\lambda_x}\} \tag{13d}$$

$$P^{(b)} \approx -\bar{\sigma}^{(e)}\{P_{c,a}^{(b)}|_{\lambda=\lambda_y} + p_{c,p}^{(b)}|_{\lambda=\lambda_x}\} \tag{14d}$$

To check the validity of such a superposition we shall consider as our first example† a spherical cap for which we know the stress coefficient exactly.

Example 1: Sphere. For this shell, the curvature is constant in all directions. Therefore, in view of Eqs. (11f) and (12f), one has

$$P_s^{(e)} \approx \bar{\sigma}^{(e)}\left\{1 + \frac{\pi\lambda^2}{64} + \frac{5\pi\lambda^2}{64}\right\} = \bar{\sigma}^{(e)}\left\{1 + \frac{3\pi\lambda^2}{32}\right\}, \qquad \lambda < 1$$

which is identical to the exact expression [see Eq. (11a)]. Similarly,

$$P_s^{(b)} \approx -\bar{\sigma}^{(e)}\frac{(3^{1/2})\lambda^2}{(1-\nu^2)^{1/2}(4-\nu_0)}\left\{\frac{42-37\nu_0}{96} + \frac{6-5\nu_0}{16}\left(\gamma + \ln\frac{\lambda}{8}\right)\right.$$
$$\left. + \frac{1+\nu}{32} + \frac{1+\nu}{16}\left(\gamma + \ln\frac{\lambda}{8}\right)\right\}$$
$$= -\bar{\sigma}^{(e)}\frac{(3^{1/2})\lambda^2}{(1-\nu^2)^{1/2}(4-\nu_0)}\left\{\frac{-0.1+5\nu}{32} + \frac{1+3\nu}{8}\left(\gamma + \ln\frac{\lambda}{4}\right)\right\},$$
$$\lambda < 1$$

which agrees fairly well with Eq. (12a). One may conclude, therefore, that such a hypothesis may not be unreasonable.

† In the following examples, we have assumed that $\bar{\sigma}^{(b)} = 0$.

Example 2: Circular conical shell (see Fig. 14). In this case, one curvature is infinite and the other finite; therefore,

$$\text{For an axial crack:} \quad P_{①}^{(e)} \approx \bar{\sigma}^{(e)}\left\{1 + \frac{5\pi}{64}\lambda_1^2\right\}, \qquad \lambda_1 < 1$$

$$P_{②}^{(e)} \approx \bar{\sigma}^{(e)}\left\{1 + \frac{5\pi}{64}\lambda_2^2\right\}, \qquad \lambda_2 < 1$$

$$\text{For a peripheral crack:} \quad P_{③}^{(e)} \approx \bar{\sigma}^{(e)}\left\{1 + \frac{\pi}{64}\lambda_3^2\right\}, \qquad \lambda_3 < 1$$

where

$$\lambda_1^2 \equiv \{12(1 - \nu^2)\}^{1/2} \frac{c^2}{(R - c\tan\epsilon)h}$$

$$\lambda_2^2 \equiv \{12(1 - \nu^2)\}^{1/2} \frac{c^2}{(R + c\tan\epsilon)h}$$

$$\lambda_3^2 \equiv \{12(1 - \nu^2)\}^{1/2} \frac{c^2}{R_3 h}$$

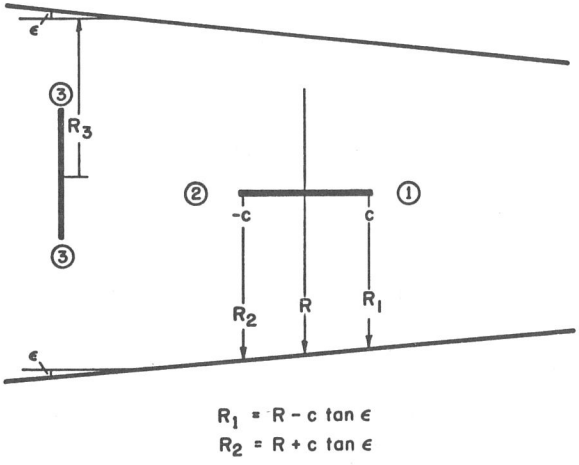

Figure 14 Circular conical shell.

Example 3: Toroidal shell (see Fig. 15). For an axial crack in the outer surface,

$$P_{①}^{(e)} \approx \bar{\sigma}^{(e)}\left\{1 + \frac{5\pi}{64}\lambda_1^2 + \frac{\pi}{64}\lambda_2^2\right\}, \qquad \lambda_{1,2} < 1$$

For an axial crack in the inner surface,

$$P_{②}^{(e)} \cong \bar{\sigma}^{(e)}\left\{1 + \frac{5\pi}{64}\lambda_1^2 - \frac{\pi}{64}\lambda_3^2\right\}, \qquad \lambda_{1,3} < 1$$

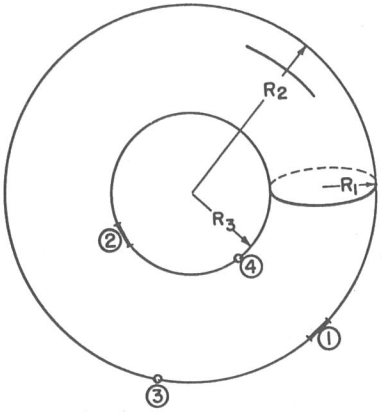

Figure 15 Toroidal shell.

For a peripheral crack in the outer surface,

$$P_{③}^{(e)} \approx \bar{\sigma}^{(e)}\left\{1 + \frac{5\pi}{64}\lambda_2^2 + \frac{\pi}{64}\lambda_1^2\right\}, \qquad \lambda_{1,2} < 1$$

For a peripheral crack in the inner surface,

$$P_{④}^{(e)} \approx \bar{\sigma}^{(e)}\left\{1 - \frac{5\pi}{64}\lambda_3^2 + \frac{\pi}{64}\lambda_1^2\right\}, \qquad \lambda_{1,3} < 1$$

DISCUSSION

In view of the above, one may conjecture that in an initially curved sheet,

1. The stresses are proportional to $(c/r)^{1/2}$.
2. The stresses have the same angular distribution as that of a flat plate.
3. The stress intensity factors are functions of the shell geometry and, in the limit, we recover the flat plate.
4. The stresses include interaction terms for bending and stretching.

A typical term is of the form

$$\frac{\sigma_{\text{shell}}}{\sigma_{\text{plate}}} \approx 1 + \left\{\frac{a_1}{R_1} + \frac{a_2}{R_2} + \frac{b_1}{R_1}\ln\frac{c}{(R_1 h)^{1/2}} + \frac{b_2}{R_2}\ln\frac{c}{(R_2 h)^{1/2}}\right\}\frac{c^2}{h} + 0\left(\frac{1}{R_1^2}, \frac{1}{R_2^2}\right) \tag{15}$$

where the expression inside the braces is a positive quantity. One concludes, therefore, that the general effect of initial curvature, in reference to that of a

flat sheet, is to increase the stresses in the neighborhood of the crack tip and reduce its resistance to fracture initiation.

It is of some practical value to be able to correlate flat sheet behavior with that of initially curved specimens. In experimental work on brittle fracture, for example, considerable time could be saved since by Eq. (15) we would expect to predict the response behavior of curved sheets from flat sheet tests.

Particular solutions

To get a better understanding of the stresses in the vicinity of a crack tip, we examine the following two illustrations:

Clamped sherical shell. Consider a clamped segment of a shallow spherical shell of base radius $\bar{R}_0$ and containing a radial crack of finite length $2c$ at the apex (see Fig. 16). The shell is subjected to a uniform internal pres-

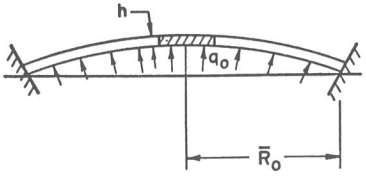

Figure 16 Pressurized spherical cap with fixed ends.

sure q_0 with radial tension $N_r = (q_0/2)R$, and, because it is clamped, we require that the displacement and slope vanish at $\bar{R} = \bar{R}_0$. For this problem the residual *applied bending* and *applied stretching* loads at the crack are† $\bar{\sigma}^{(b)} = 0$ and $\bar{\sigma}_e = q_0 R/2h$. Along the crack prolongation one finds from Eqs. (6), (11a), and (12a) that the stress normal to the crack is

$$\sigma_n(x, 0)|_{\nu=1/3} \approx \left(\frac{c}{2r}\right)^{1/2} \{1 + (0.47 - 0.46 \ln \lambda)\lambda^2\} \frac{q_0 R}{2h} \tag{16a}$$

which for $\lambda = 1$ reduces to

$$\sigma_n(x, 0) \approx 1.48 \left(\frac{c}{2r}\right)^{1/2} \frac{q_0 R}{2h} \tag{16b}$$

Closed cylindrical tank. Consider a shallow cylindrical shell containing a crack of length $2c$. The shell is subjected to a uniform internal pressure q_0 with an axial tension $N_x = (q_0 R/2)$, $M_y = 0$, far away from the crack. For this problem, if the crack is parallel to the axis of the cylinder, then $\bar{\sigma}^{(b)} = 0$ and $\bar{\sigma}^{(e)} = (q_0 R/h)$. Hence the normal stress along the crack prolongation

† For details, see Folias, 1965c.

can be found from Eqs. (6), (11c), and (12c), and is

$$\sigma_n(x, 0)|_{\nu=1/3} \approx \left(\frac{c}{2r}\right)^{1/2}\{1 + (0.37 - 0.30 \ln \lambda)\lambda^2\}\frac{q_0 R}{h} \tag{17a}$$

which for $\lambda = 1$ reduces to

$$\sigma_n(x, 0) \approx 1.37\left(\frac{c}{2r}\right)^{1/2}\frac{q_0 R}{h} \tag{17b}$$

If the crack is perpendicular to the axis of the cylinder, then $\bar{\sigma}^{(b)} = 0$ and $\bar{\sigma}^{(e)} = q_0 R/2h$; therefore,

$$\sigma_n(x, 0)|_{\nu=1/3} = \left(\frac{c}{2r}\right)^{1/2}\{1 + (0.20 - 0.15 \ln \lambda)\lambda^2\}\frac{q_0 R}{2h} \tag{18a}$$

which for $\lambda = 1$ reduces to

$$\sigma_n(x, 0) \approx 1.20\left(\frac{c}{2r}\right)^{1/2}\frac{q_0 R}{2h} \tag{18b}$$

In the event that the crack makes an angle α with the axis of the cylinder, then $\bar{\sigma}^{(b)} = 0$, $\bar{\sigma}^{(e)} = (q_0 R/4h)(3 + \cos 2\alpha)$, $\bar{\tau}^{(e)} = (q_0 R/4h) \sin 2\alpha$. Thus the normal to the crack stress may be derived from Eqs. (6), (11e), and (12e).

A FRACTURE CRITERION

Elastic considerations

It is well known that large, thin-walled pressure vessels resemble balloons and like balloons are subject to puncture and explosive loss. For a given material, under a specified stress field due to internal pressure, there will be a crack length in the material which will be self-propagating. Crack lengths less than the critical value will cause leakage but not destruction. However, if the critical length is ever reached, either by penetration or by the growth of a small fatigue crack, an explosion and complete loss of the structure may occur. The subject of eventual concern therefore is to assess analytically the relation between critical pressure and critical crack lengths in sheets which are initially curved.

The principal task of fracture mechanics is precisely the prediction of such failure in the presence of sharp discontinuities, on the basis of geometry, material behavior, etc. Specifically, the approach is based on a corollary of the first law of thermodynamics which was first applied to the phenomenon of fracture by Griffith (1924), whose hypothesis was that the total energy of a cracked system subjected to loading remains constant as the crack extends an infinitesimal distance. It should, of course, be recognized that this is a necessary, but not sufficient condition for failure.

Griffith applied his criterion to the stretching of an infinite isotropic plate containing a flat, sharp-ended crack of length $2c$, and showed that the criterion can be expressed in terms of an integral over the entire surface of the plate. Subsequently, Sanders (1960) has proved that this integral is independent of the path; i.e., one may integrate along any simple contour enclosing the crack.

Following similar lines, Folias (1970) derived the following approximate criterion which is applicable to thin, shallow shells:

$$\frac{(33 + 6\nu - 7\nu^2)(1 + \nu)}{3(9-7\nu)}[p^{(b)}]^2 + [p^{(e)}]^2 = \frac{16G\gamma^*}{c\pi}\frac{2(1 + \nu)}{9 - 7\nu} \equiv (\sigma_F)^2 \qquad (19)$$

Geometrically, this equation represents a family of ellipses whose semimajor and semiminor axes are, respectively,

$$\{\sqrt{3(9 - 7\nu)}(4 - \nu_0)/\sqrt{(1 + \nu)(33 + 6\nu - 7\nu^2)}\}\sigma_F \qquad \text{and} \qquad \sigma_F$$

Plasticity correction

Due to the presence of high stresses in the vicinity of the tip of a crack; when a yield criterion is satisfied, some localized plastic deformation occurs and a plastic zone is created. This phenomenon effectively increases the crack length and therefore must be accounted for. Following Dugdale (1960) the size of the plastic zone (see Fig. 17) is determined by the relation

$$\frac{c}{c_e} = \cos\left(\frac{\pi\sigma}{2\sigma_\gamma}\right) \qquad (20)$$

or

$$\frac{\rho}{c} = \sec\left(\frac{\pi}{2}\frac{\rho}{\sigma_\gamma}\right) - 1 \qquad (21)$$

This relation applies only to a perfect elastic-plastic non-strain-hardening material. McClintock (1961), however, has suggested that a strain-hardening material may be approximated by an ideally plastic one if a stress higher than σ_γ and lower than σ_u is chosen. Subsequently, Hahn and Rosenfield (1965) suggested that σ_γ in Eq. (20) be replaced by $\sigma^* = (\sigma_u + \sigma_\gamma)/2$. Thus, correcting the Griffith-Irwin equation so as to include yielding and geometry effects, one has†

† For a derivation of this equation, applicable to flat plates, see Tetelman and McEvily (1967). A more realistic approach would be to treat σ^* and K as floating constants to be determined such that Eq. (22) presents "a best fit." One may, however, choose for σ^* the value suggested by Hahn and Rosenfield or the alternative value suggested by the author: $\{\sigma_\gamma + [(\sigma_\gamma + \sigma_u)/2]\}/2$.

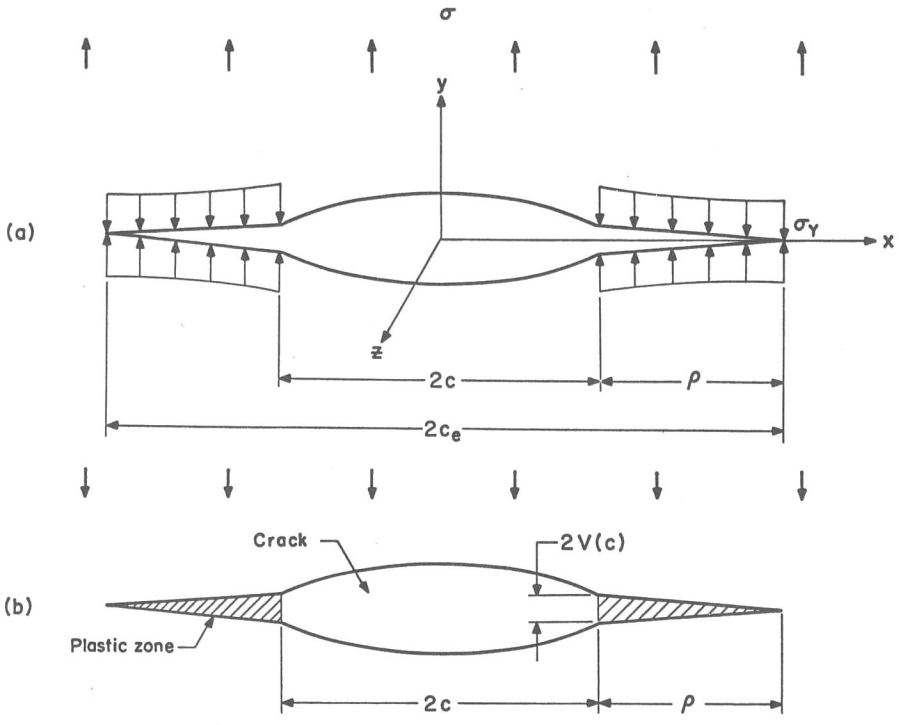

Figure 17 (a) Internal stress distribution used in the Dugdale model of elastic-plastic deformation near a crack of length $2c$ under plane-stress tensile loading. (b) Displacements $2V$ associated with crack opening. *After Hahn and Rosenfield, 1965.*

$$\sigma_F = \frac{2\sigma^*}{\pi} \cos^{-1}\left[\exp\left(-\frac{\pi K^2}{8\sigma^{*2}c}\right)\right] \tag{22}$$

which upon substituting for σ_F from Eq. (19) now reads

$$\bar{\sigma}^{(e)}\left\{\frac{(33 + 6\nu - 7\nu^2)(1 + \nu)}{3(9 - 7\nu)}[P^{(b)}]^2 + [P^{(e)}]^2\right\}^{1/2} = \frac{2\sigma^*}{\pi} \cos^{-1}\left[\exp\left(-\frac{\pi K^2}{8\sigma^{*2}c}\right)\right] \tag{23}$$

It should be emphasized that this criterion is not valid after general yield. At the present time there are no adequate criteria to handle these problems. Also, in deriving Eq. (23) we have assumed that the plastic zone sizes ahead of the crack tip for initially curved sheets may be approximated by Eq. (20). Such an approximation simplifies the general criterion considerably† and is valid for $\sigma_F < 0.95\sigma^*$.

† For a more accurate but more complex criterion, see the last section.

COMPARISON BETWEEN THEORY AND EXPERIMENTS‡

In judging the adequacy of a theory, one often compares theoretical and experimental results. Therefore, in the following we compare our results with some of the experimental data existing in literature.

However, to use Eq. (23) one must know a priori the fracture toughness K. This difficulty can be eliminated if one proceeds in the following manner: (1) use the test data and compute the Ks, (2) find the average K, and (3) use the K_{av} to predict failure hoop stresses.

R. C. Aungst, Additional crack propagation tests on zircaloy-2 pressure tubes. Electrotech. Technol. Vol. 4, No. 7-8 (July/ Aug. 1966). This paper gives results of tests on a 2.7-in.-diameter, 0.26-in.-thick N-reactor tube with v-shaped cracks.

Material: 30% cold-drawn zircaloy-2
σ_y: 98.0 ksi, $\sigma^* = 98.4$ ksi
σ_u: 98.6 ksi, $K = 240.0$ ksi-$\sqrt{\text{in}}$

The results are plotted in Fig. 18. Notice that the agreement is very good for large crack lengths. However, for small crack lengths the predicted values are somewhat lower. This is not contrary to our expectations since our calculations were based on through-the-thickness cracks.

R. P. Sopher, A. L. Lowe, D. C. Martin, and P. J. Rieppel, Evaluation of weld joint flaws on initiating points of brittle fracture, Welding J. (Nov. 1959), p. 4415. The results of tests on 9-ft-diameter, $\frac{3}{4}$-in.-thick spheres with full thickness cracks are given.

Material: ABS-B Steel
σ_y: 30.7 ksi, $\sigma^* = 37.9$ ksi
σ_u: 59.4 ksi, $K = 102.0$ ksi-$\sqrt{\text{in}}$

The results are plotted in Fig. (19). The agreement is very good.

R. B. Anderson and T. L. Sullivan, Fracture mechanics of through-cracked cylindrical pressure vessels. NASA TN D-3252. This paper gives results of tests on 6-in.-diameter, 0.060-in.-thick cylinders with full thickness cracks.

1. Material: 2014-T6Al
σ_y: 90.5 ksi, $\sigma^* = 91.9$ ksi
σ_u: 93.9 ksi, $K = 51.6$ ksi-$\sqrt{\text{in}}$

‡ See Quirk (1967) and Folias (1969a).

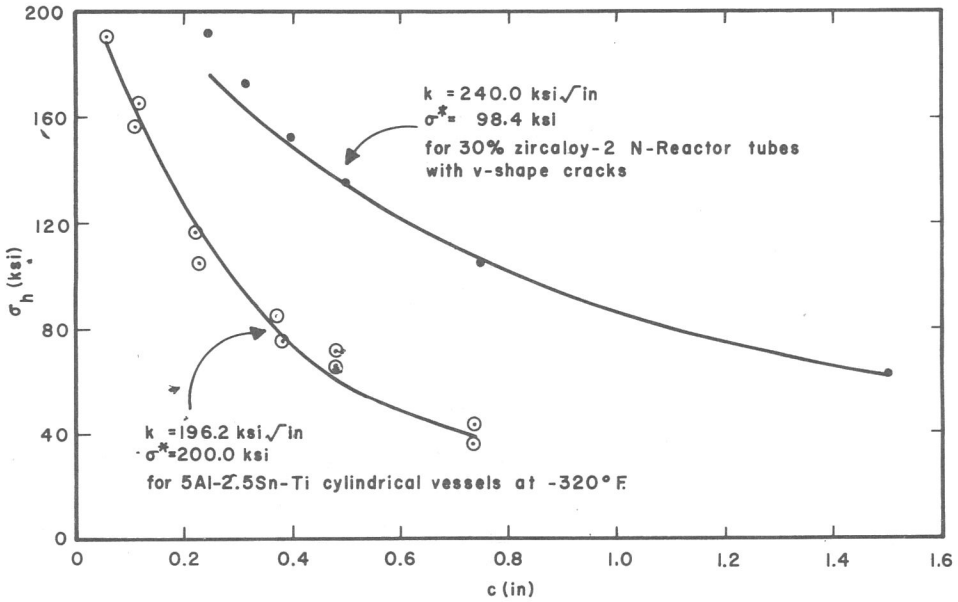

Figure 18 Comparison between theory and experiment.

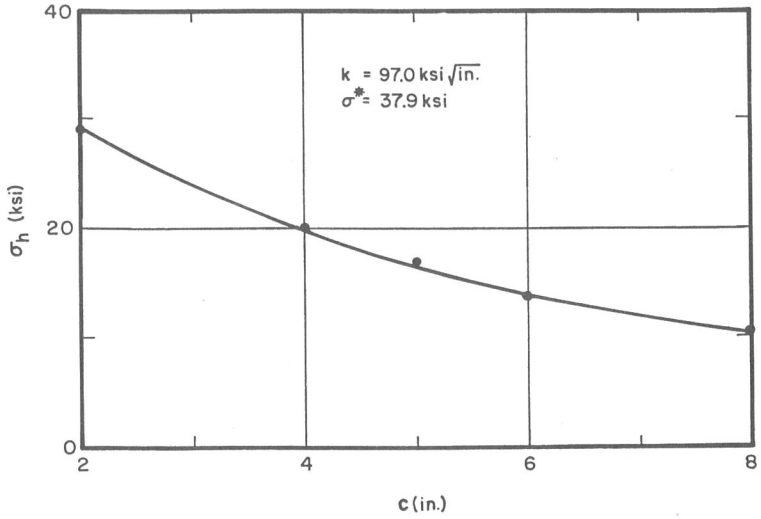

Figure 19 Comparison between theory and experiment for ABS-B steel spherical vessels.

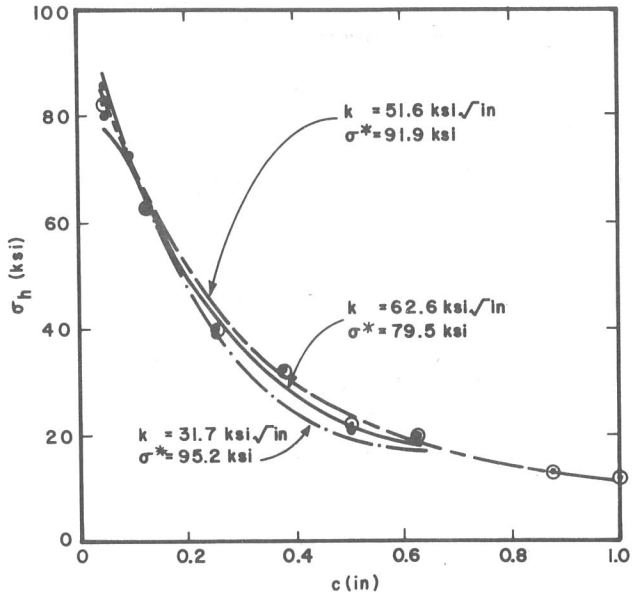

Figure 20 Comparison between theory and experiment for 2014-T6A1 cylindrical vessels at −423°F.

The results are plotted in Fig. (20). The agreement is good.

2. Material: 2014-T6A1
   σ_y: 82.0 ksi, $\sigma^* = 85.0$ ksi
   σ_u: 93.9 ksi, $K = 48.6$ ksi-$\sqrt{\text{in}}$

The results are plotted in Fig. (21). The agreement is good.

3. Material: 2014-T6A1
   σ_y: 68.0 ksi, $\sigma^* = 70.8$ ksi
   σ_u: 79.0 ksi, $K = 43.4$ ksi-$\sqrt{\text{in}}$

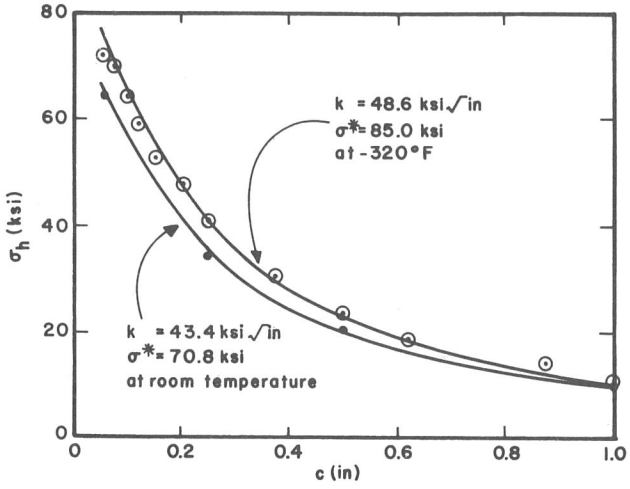

Figure 21 Comparison between theory and experiment for 2014-T6A1 cylindrical vessels.

The results are plotted in Fig. (21). The agreement is good.

Results of tests on 6-in.-diameter, 0.020-in.-thick cylinders with full thickness cracks are also given.

4. Material: 5A1-2.5S_n-Ti
   σ_{yB}: 222 ksi, $\sigma^* = 200$ ksi
   σ_u: not specified, $K = 196$ ksi-$\sqrt{\text{in}}$

The results are plotted in Fig. (18). The agreement is fairly good. It should be pointed out that titanium alloys exhibit significant increase in biaxial yield strength relative to uniaxial yield strength. Hence the von Mises yield criterion may or may not be applicable. Be that as it may, if one uses a σ^* slightly less than 200 ksi, even better agreement is noticed.

T. E. Taylor and F. M. Burdekin, Unstable fracture by the shear mode in spherical vessels with long flaws. B.W.R.A. C157/2/66. Results of tests on 58-in.-diameter, 0.50-in.-thick spheres with through thickness cracks are given.

Material: B.S. 1501-161: 1958, Grade B
σ_y: 36.0 ksi at 80°C, $\sigma^* = 42.2$ ksi
σ_u: 60.9 ksi at 80°C, $K = 200.0$ ksi-$\sqrt{\text{in}}$

The results are plotted in Fig. (24). The agreement is good except at one point, but this is due to a temperature change.

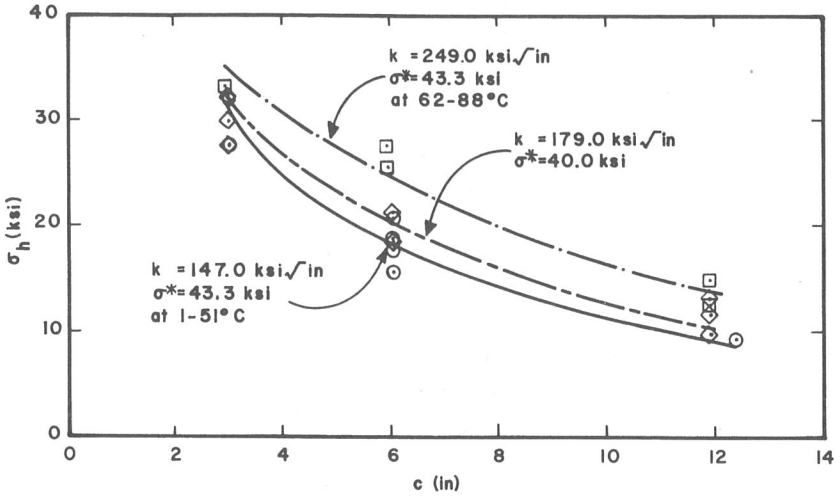

Figure 22 Comparison between theory and experiment for 0.36% C steel cylindrical vessels.

W. H. Irvine, A. Quirk and E. Bevitt, Fast fracture of pressure vessels: An appraisal of theoretical and experimental aspects and application to operational safety. J. Brit. Nucl. Energy Soc. (Jan. 1964). The results of tests on 5-ft-diameter, 1-in.-thick, cylindrical vessels with through cracks are given.

Material: 0.36% C Steel
σ_y: 33 ksi, $\sigma^* = 40$ ksi
σ_u: 61 ksi, $K = 179$ ksi-$\sqrt{\text{in}}$

The results are plotted in Fig. (22). The agreement is fairly good.

D. L. Getz, W. S. Pierce, and H. F. Calvert, Correlation of uniaxial notch tinsile data with pressure vessel fracture characteristics. ASME Paper

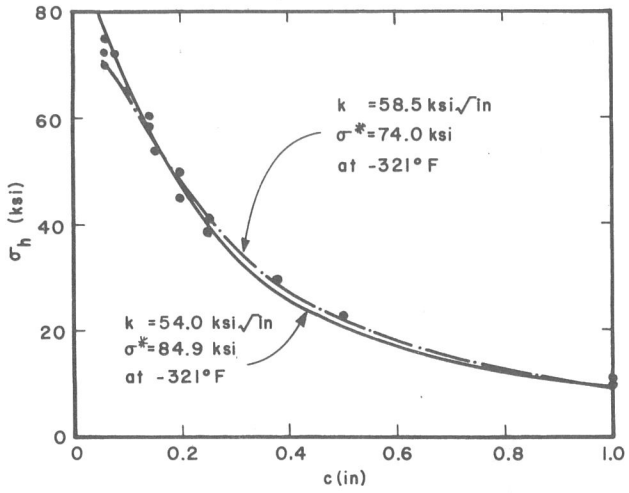

Figure 23 Comparison between theory and experiment for 2014-T6A1 cylindrical vessels.

63-WA-187. This paper shows results of tests on 3-in.-diameter, 0.060-in.-thick cylindrical vessels with through cracks.

1. Material: 2014-T6 aluminum alloy
   σ_y: 81.9 ksi, $\sigma^* = 84.9$ ksi
   σ_u: 93.9 ksi, $K = 54.0$ ksi-$\sqrt{\text{in}}$

The results are plotted in Fig. (23). The agreement is fairly good. Note that Folias (1967) does not make it clear as to whether $\sigma_y = 81.9$ ksi is the biaxial or uniaxial yield stress. If, however, it represents the biaxial yield stress, then $\sigma^* = 74$ ksi and $K = 58.5$ ksi-in.^{2} and the agreement is even better (see Fig. 23).

2. Material: 2014-T6 aluminum alloy
   σ_y: 90.8 ksi, $\sigma^* = 95.2$ ksi
   σ_u: 108.4 ksi, $K = 51.7$ ksi-$\sqrt{\text{in}}$

The results are plotted in Fig. (20). The agreement is not very good. Here again the same remark as in part 1 holds. Thus if one uses $\sigma^* = 79.5$ ksi and $K = 62.6$ ksi-in.^{2}, the agreement is better (see Fig. 20).

A. R. Duffy, Studies of hydrostatic test levels and defect behavior. In Symp. on Line Pipe Res., Pipeline Research Committee of American Gas Association, Dallas, November 17–18, 1965. The results of tests on 30-in.-diameter, $\frac{3}{8}$-in.-thick pipes with through cracks are given.

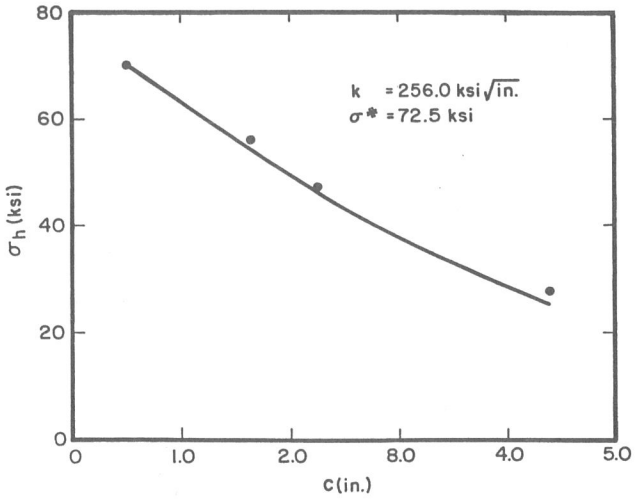

Figure 24 Comparison between theory and experiment for B.S. 1501–161: 1958 Grade B spherical vessels.

Material: X-52 plain carbon (semikilled)

σ_y: 56 ksi, $\sigma^* = 73$ ksi

σ_u: 78 ksi, $K = 256$ ksi-$\sqrt{\text{in}}$

The results are plotted in Fig. (25). The agreement is good.

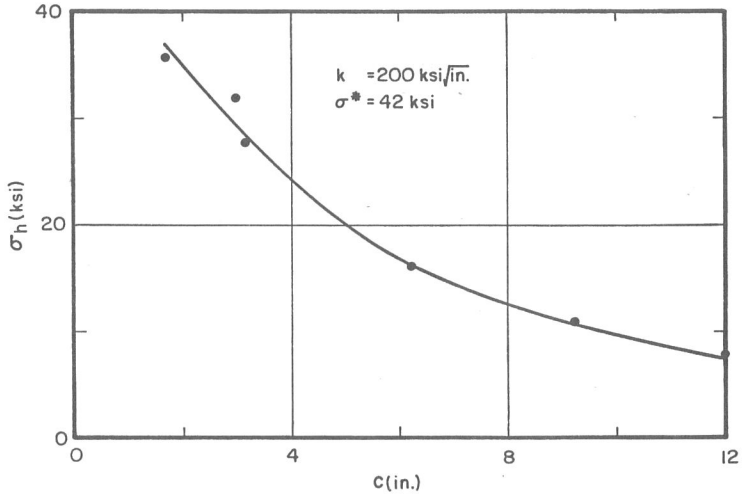

Figure 25 Comparison between theory and experiment for X-52 plain carbon pipes.

R. W. Nichols, W. H. Irvine, A. Quirk, and E. Bevitt, A limit approach to the presentation of pressure vessel failure. Proc. First Intern. Conf. on Fracture, Sendai, Japan, 1673, 1966.

Material: 0.36 C Steel

σ_y: 34.5 ksi, $\sigma^* = 43.3$ ksi

σ_u: 69.5 ksi $K = 249.0$ ksi-$\sqrt{\text{in.}}$

The results are plotted in Fig. (22). The agreement is fairly good. There is some temperature variation which effects to some extent the fracture toughness K.

ESTIMATING PLASTIC ZONE SIZES

Inasmuch as the Dugdale model (1960) is an approximate model for a pseudo-elastoplastic analysis, the following simple method for estimating plastic zone sizes ahead of the crack tip is somewhat justifiable.

Plastic zone size for a plate

Consider the tensile stress σ as acting on a thin plate containing a crack of length $2c_e$. Then the singular term of the stress $\sigma_y^{(1)}$ along the crack prolongation at $x = c_e + r$ is

$$\sigma_y^{(1)} = \sigma\sqrt{\frac{c+\rho}{2r}} + \cdots \tag{24}$$

Consider next the yield compressive stress as acting on a thin plate containing a crack of length 2ρ. Similarly, the singular term of the stress $\sigma_y^{(2)}$ at the same point $x = c_e + r$ is

$$\sigma_y^{(2)} = -\sigma_y\sqrt{\frac{\rho}{2r}} + \cdots \tag{25}$$

Superimposing the two solutions and requiring that the stress σ_y be finite give

$$\sigma\sqrt{\frac{c+\rho}{2r}} - \sigma_y\sqrt{\frac{\rho}{2r}} = 0 \tag{26}$$

or

$$a \equiv \frac{c}{c_e} = 1 - \left(\frac{\sigma}{\sigma_y}\right)^2 \tag{27}$$

A comparison between the experimental and the theoretically predicted values is given in Fig. 26.

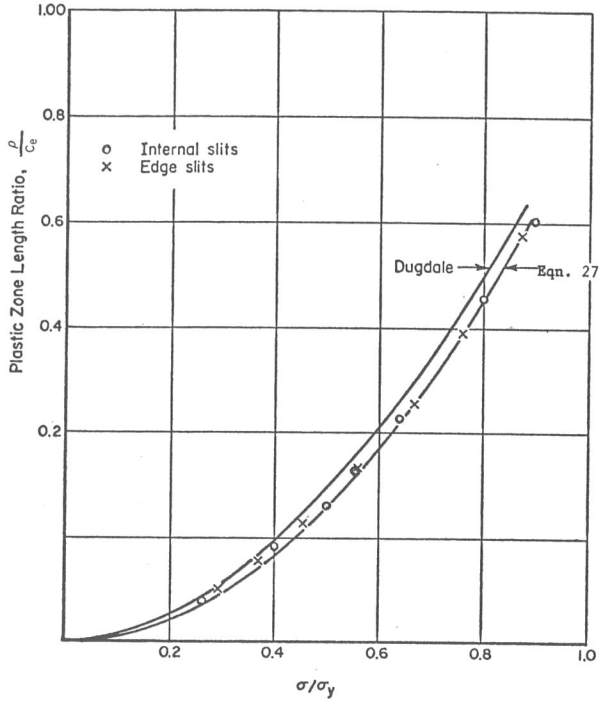

Figure 26 Comparison of plastic zone lengths.

PLASTIC ZONE SIZE FOR A CYLINDRICAL SHELL (AXIAL CRACK)

Proceeding along the same lines, one, in view of Folias, 1965a, has

$$\sigma_h A_{c,a}^{(e)}(c_e)\sqrt{\frac{c_e}{2r}} - \sigma_y A_{c,a}^{(e)}(\rho)\sqrt{\frac{\rho}{2r}} = 0 \tag{28}$$

where the geometry correction factor $A_{c,a}^{(e)}(c)$ is given by Table 2 and may be approximated within a 6% error by

$$A_{c,a}^{(e)}(c) \simeq \sqrt{1 + 0.34\lambda^2} \tag{29}$$

Solving Eq. (28) for the ratio a, one has

$$a \equiv \frac{c}{c_e} = 1 - \left(\frac{\sigma_h}{\sigma_y}\right)^2 \frac{1 + 0.34\lambda^2(1/a)^2}{1 + 0.34\lambda^2[(1/a) - 1]^2} \tag{30}$$

It is interesting to note that Eq. (30) agrees well with the exact results recently obtained by Erdogan and Ratwani, 1972, after long and difficult calculations.

Crack opening displacement

It is clear that as the plastic zones spread from the tip of the crack, the crack opening displacements $2V(c)$ produced at the tip will increase. These displacements, in the case of a plate, are related to the plastic zone size ρ by

$$2V(c) = \frac{8\sigma_y c}{\pi E} \ln\left(\frac{c_e}{c}\right) \tag{31}$$

One may conjecture, therefore, that the crack opening displacement for a cylindrical shell will be of a similar form except for an appropriate geometry correction factor, in particular

$$2V(c) = \frac{8\sigma_y c}{\pi E} A_{c,a}^{(e)}(c_e) \ln\left(\frac{c_e}{c}\right) \tag{32}$$

Again, comparing Eq. (32) with the results of Erdogan and Ratwani, 1972, one finds a fairly good agreement.

Fracture criterion

If we adopt, therefore, the criterion that for the initiation of an unstable fracture near the tip of a slowly moving crack (Tetelman and McEvily, 1967),

$$\frac{K^2}{2E} = \sigma_y V^*(c) \tag{33}$$

where $V^*(c)$ represents the critical value of $V(c)$, one finds that

$$K^2 = \frac{8\sigma_y^2 c}{\pi} A_{c,a}^{(e)}(c_e) \ln\left(\frac{c_e}{c}\right) \tag{34}$$

Subsequently, upon using Eq. (27) and upon solving for the hoop stress, one derives the following fracture criterion†:

$$\frac{\sigma_h}{\sigma_y} = \frac{A_{c,a}^{(e)}(c_e - c)}{A_{c,a}^{(e)}(c_e)} \sqrt{1 - \exp\left(\frac{\pi K^2}{8\sigma_y^2 c}\right)} \tag{35}$$

It should be pointed out that in using Eq. (35) one does not know a priori the effective crack length c_e; therefore, a successive approximation scheme should be used until both Eq. (30) and Eq. (35) are satisfied simultaneously‡,

† For a strain hardening material, replace σ_y by σ^*; for other shell geometries, replace A by the coefficient $P^{(e)}$.

‡ It can be shown that there exists only one $c_e > c$ that satisfies the two equations.

Although this criterion will yield more accurate results, it is not of much practical value because of the lengthy calculations that must be carried out.

CONCLUSION

The close agreement between the theoretically predicted fracture strengths and the experimental data suggests that Eq. (23) may be used to predict failures in pressurized vessels knowing only the structural geometry, the crack length, the ultimate and yield stresses, and the fracture toughness of the material.

Finally, for such materials where the fracture hoop stress is close to the σ^* value, one should use the more accurate yet more difficult criterion, i.e., Eq. (35).

DISCUSSION

In view of Chapter 22, the following question may arise. If classic theory is so inadequate, then why does it agree so well with experiments?

First of all, it is true that classic theory is inadequate in predicting the exact bending stresses in the vicinity of a crack. However, in general, these bending stresses are very small when compared (in the vicinity of crack) with the extensional stresses and therefore may be neglected. In fact, in all the above comparisons between classic theory and experiments this was the case. On the other hand, for very long cracks such contributions become significant and therefore can no longer be neglected. Unfortunately in such cases bulging effects become extremely important and any theory, whether classic or *shear*, is inadequate.

As for the difference between the two theories in predicting the extensional stresses (see Fig. 6 of Chapter 22), there is a question in the author's mind as to how meaningful such a comparison is. Specifically, according to Ogibalov a shell is thin if $h/R \leq 0.01$ and therefore any results beyond this range must be used with extreme caution.

Be that as it may, one may conjecture that qualitatively the same character of the solution prevails and therefore the fracture criterion [Eq. (23)] treating σ^* and K as floating constants to be determined from scaled-down models may still be used (see the footnote on p. 503).

Acknowledgment: *This work was supported in part by the National Science Foundation, Grant No. GK-1440, and by Edwards Air Force Base, Contract No. F04611-67-C-0043.*

LIST OF SYMBOLS

$A_s^{(e)}, A_{c,a}^{(e)}, A_s^{(b)}, A_{c,a}^{(b)}, a_s^{(e)}, a_{c,a}^{(e)}, a_s^{(b)}, a_{c,a}^{(b)}$	as defined in test
a	$\frac{c}{c_e}$
c	half crack length
$c_e \equiv c + \rho$	half effective crack length
$D \equiv Eh^2/[12(1 - \nu^2)]$	flexural rigidity
E	Young's modulus
$F(x, y)$	stress function
G	shear modulus
h	thickness
K	fracture toughness (for flat plates)
L	linear dimension
$P_s^{(e)}, P_p^{(e)}, P_{c,a}^{(e)}, P_{c,c}^{(e)}, P_{c,\alpha}^{(e)}, P_{①}^{(e)}, P_{②}^{(e)}, P_{③}^{(e)}, P_{④}^{(e)}, P_s^{(b)}, P_p^{(b)}, P_{c,a}^{(e)}, P_{c,c}^{(e)}, P_{c,\alpha}^{(e)}$	stress coefficients as defined in text
$q(x, y)$	internal pressure
q_0	uniform internal pressure
R, R_x, R_y, R_1, R_2	radii of an initially curved sheet
$r = \sqrt{(x - c)^2 + y^2}$, $\theta = \tan^{-1}[y/(x - c)]$	polar coordinates
$2V(c)$	crack opening displacement
$w(x, y)$	displacement function
$w_0(x, y)$	initial displacement function
x, y, z	rectangular Cartesian coordinates
α	orientation angle as defined in Fig. 13
γ	0.5768 . . . = Euler's constant
γ^*	surface energy per unit area
ϵ	as defined in Fig. 14
λ^4	$\frac{Ehc^4}{R^2D} = \frac{12(1 - \nu^2)c^4}{R^2h^2}$
$\lambda_1, \lambda_2, \lambda_3, \lambda_x, \lambda_y$	as defined in text
ν	Poisson's ratio
ν_0	$1 - \nu$
π	3.14 . . .
ρ	size of plastic zone
σ	normal stress as defined in Fig. 17
σ_y	uniaxial yield stress
σ_u	ultimate stress
σ^*	$\frac{\sigma_y + (\sigma_y + \sigma_u/2)}{2}$

σ_F	fracture stress
σ_h	hoop stress
σ_n	normal to the crack stress evaluated just ahead of the crack prolongation
$\sigma_x^{(e)}, \sigma_y^{(e)}, \tau_{xy}^{(e)}$	stretching stress components
$\sigma_x^{(b)}, \sigma_y^{(b)}, \tau_{xy}^{(b)}$	bending stress components
$\bar{\sigma}^{(e)}$	applied stretching stress
$\bar{\sigma}^{(b)}$	applied bending stress
$\bar{\tau}^{(e)}$	applied in-plane shear
$\bar{\tau}^{(b)}$	applied equivalent shear
∇^2	Laplacian operator
∇^4	biharmonic operator

REFERENCES

Copley, L. G., Sanders, J. L., 1969. Longitudinal crack in a cylindrical shell under internal pressure. *Intern. J. Fracture Mech.* 5: 117–131.

Dugdale, D. S., 1960. Yielding of steel sheets containing slits. *J. Mech. Phys. Solids* 8: 100–104.

Duncan, M. E., Sanders, J. L., 1969. The effect of a circumferential stiffness on the stress in a pressurized cylindrical shell with a longitudinal crack. *Intern. J. Fracture Mech.* 5: 133–155.

Erdogan, F., Kibler, J., 1969. Cylindrical and spherical shells with cracks. *Intern. J. Fracture Mech.* 5: 229–237.

Erdogan, F., Ratwani, M., 1972. Plasticity and the crack opening displacement in shells. *Intern. J. Fracture Mech.* 8: 413–426.

Folias, E. S., 1964a. The stresses in a spherical shell containing a crack. *ARL 64-23.* Aerospace Research Laboratories, U.S. Air Force, Dayton, Ohio.

Folias, E. S., 1964b. The stresses in a cylindrical shell containing an axial crack. *ARL 64-174*, Aerospace Research Laboratories, U.S. Air Force, Dayton, Ohio.

Folias, E. S., 1965a. The stresses in a cracked spherical shell. *J. Math. Phys.*, 5: 327–346.

Folias, E. S., 1965b. A finite line crack in a pressurized spherical shell. *Intern. J. Fracture Mech.* 1: 104–113.

Folias, E. S., 1965c. An axial crack in a pressurized cylindrical shell. *Intern. J. Fracture Mech.* 1: 20–46.

Folias, E. S., 1967. A circumferential crack in a pressurized cylindrical shell. *Intern. J. Fracture Mech.* 3: 1–11.

Folias, E. S., 1969a. On the prediction of failure in pressurized vessels. *First Intern. Conf. on Pressure Vessel Technol.* Delft, Netherlands, pp. 781–791.

Folias, E. S., 1969b. On the effect of initial curvature on cracked flat sheets. *Intern. J. Fracture Mech.* 5: 327–346.

Folias, E. S., 1970. On the theory of fracture of curved sheets. *Eng. Fracture Mech. J.*, 2: 151–164.

Griffith, A. A., 1924. The theory of rupture. *Proc. 1st Intern. Congr. on Appl. Mech.*, Delft, pp. 55–63.

Hahn, G. T., Rosenfield, A. R., 1965. Local yielding and extension of a crack under plane stress. *Acta Met.* 13: 293–306.

Marguerre, K., 1938. Zur Theorie Der Gekrummten Platte Grosser Formanderung. *Proc. 5th Intern. Congr. on Appl. Mech.*, pp. 93–101.

McClintock, F. A., 1961. On notch sensitivity. *Welding J. Res. Supplement* 26: 202–208.

Ogibalov, P. M., 1966. *Dynamics and Strength of Shells.* Translated from Russian, published for NASA and NSF by the Israel Program for Scientific Translations, pp. 1–45.

Quirk, A., 1967. A maximum stress theory for the failure of pressure components containing through thickness defects. *AHSB (S) R 134.* United Kingdom Atomic Energy Authority.

Sanders, J. L., 1960. On the Griffith-Irwin fracture theory. *J. Appl. Mech.* E 27: 352–353.

Sechler, E. E., Williams, M. L., 1959. The critical crack length in pressurized monocoque cylinders. *Final Rept. GALCIT 96.* California Inst. of Tech. See also Williams, M. L., 1961. *Proc. Crack Propagation Symp.* Cranfield, England. 1: 130–165.

Tetleman, A. S., McEvily, A. J., 1967. *Fracture of Structural Materials.* Wiley, New York, pp. 62–79.